Nucleic Acids Research, 2006, Vol. 34, No. 6 ***1785–1797***
doi:10.1093/nar/gkl109

Experimental and computational investigations of Ser10 and Lys13 in the binding and cleavage of DNA substrates by *Escherichia coli* DNA topoisomerase I

Daniel Strahs[1], Chang-Xi Zhu, Bokun Cheng, Jason Chen[1] and Yuk-Ching Tse-Dinh*

Department of Biochemistry and Molecular Biology, New York Medical College Valhalla, NY 10595, USA and [1]Department of Biology and Health Sciences, Pace University, New York, NY 10038, USA

Received January 3, 2006; Revised February 1, 2006; Accepted March 8, 2006

ABSTRACT

Ser10 and Lys13 found near the active site tyrosine of *Escherichia coli* DNA topoisomerase I are conserved among the type IA topoisomerases. Site-directed mutagenesis of these two residues to Ala reduced the relaxation and DNA cleavage activity, with a more severe effect from the Lys13 mutation. Changing Ser10 to Thr or Lys13 to Arg also resulted in loss of DNA cleavage and relaxation activity of the enzyme. In simulations of the open form of the topoisomerase–DNA complex, Lys13 interacts directly with Glu9 (proposed to be important in the catalytic mechanism). This interaction is removed in the K13A mutant, suggesting the importance of lysine as either a proton donor or a stabilizing cation during strand cleavage, while the Lys to Arg mutation significantly distorts catalytic residues. Ser10 forms a direct hydrogen bond with a phosphate group near the active site and is involved in direct binding of the DNA substrate; this interaction is disturbed in the S10A and S10T mutants. This combination of a lysine and a serine residue conserved in the active site of type IA topoisomerases may be required for correct positioning of the scissile phosphate and coordination of catalytic residues relative to each other so that DNA cleavage and subsequent strand passage can take place.

INTRODUCTION

Topoisomerases are enzymes that couple the cleavage of either a single- or double-strand of DNA with DNA strand passage through the break before religation of DNA phosphodiester linkage, thus catalyzing the interconversions of DNA topoisomers. *Escherichia coli* DNA topoisomerase I is a well-studied example of the type IA family of DNA topoisomerases which break a single strand of DNA in its mechanism (1,2). Its major physiological role is the removal of excessive negative supercoiling from chromosomal DNA (3–5). It is encoded by the *topA* gene for a protein of 97 kDa (6). The first step of its mechanism of action is the non-covalent binding of a single strand of DNA at its active site. Tyr319 then acts as a nucleophile to attack a scissile phosphate on the phosphodiester backbone bound at the active site, and is covalently linked via its side chain to the 5′-phosphate of the cleaved DNA in the covalent intermediate (7). The 3′ oxygen on the scissile phosphate is the leaving group. The enzyme then has to undergo conformational change to allow passage of the complementary DNA strand through the break to take place before the displaced 3′-hydroxyl group of the cleaved DNA acts as a nucleophile to attack the phosphotyrosine linkage in the religation step of the reaction. The linking number of DNA increases by one as a result of each cycle of enzyme action.

The crystal structure of the N-terminal 67 kDa transesterification domain of this enzyme has been reported (8). Potential catalytic roles for a number of conserved residues found near the active site tyrosine have been explored in previous studies by site-directed mutagenesis. Glu9 appears to be required for DNA cleavage (9,10), and there is evidence for the acidic triad of Asp111, Asp113 and Glu115 being involved in Mg(II) binding (8,11). Glu9, Asp111 and Asp113 are residues conserved in the Toprim catalytic domain found in type IA and II topoisomerases, as well as other DnaG-type primases and OLD family nucleases and may have common functions in these different nucleotidyl transfer mechanisms (12). A role for the positively charged side chain of Arg321 in stabilization of the phenolate anion during nucleophilic attack has also been proposed (9,13). His365 has been proposed to participate in DNA binding and stabilize the orientation of active site residues (14). The potential catalytic roles of other residues

*To whom correspondence should be addressed. Tel: +1 914 594 4061; Fax: +1 914 594 4058; Email: yuk-ching_tse-dinh@nymc.edu

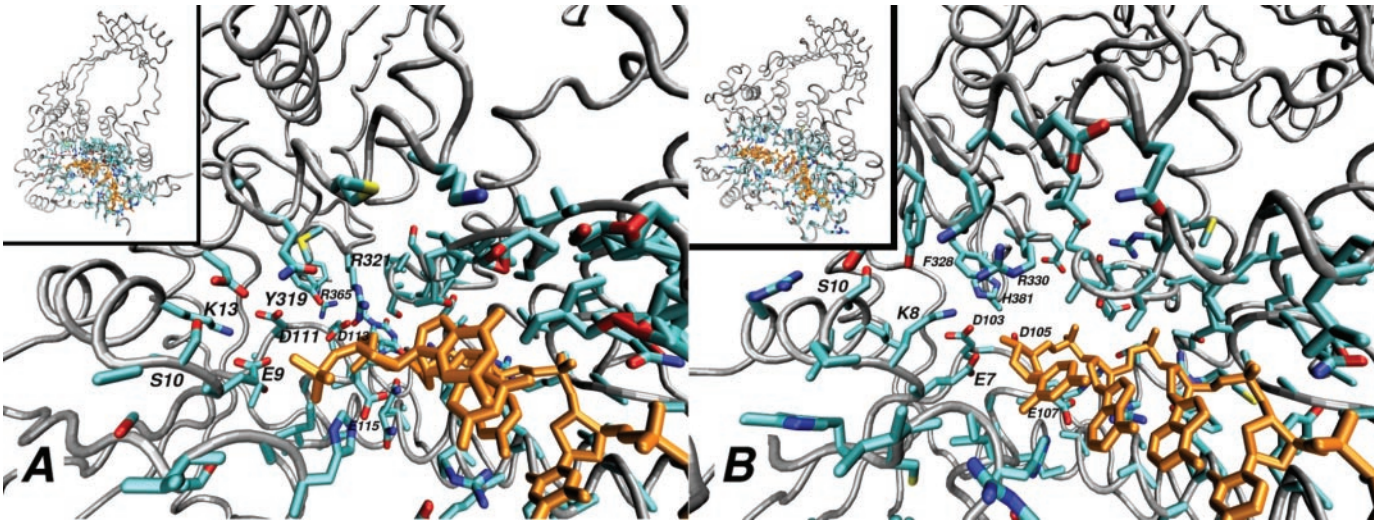

Figure 1. Structures of *E.coli* topoisomerase I and topoisomerase III. (**A**) Active site of topoisomerase I–ssDNA complex. (**B**) Active site of topoisomerase III–ssDNA complex. Residues within 10 Å of the DNA substrate are shown; only residues discussed in the text are labeled. The structure of topoisomerase I [1MW8 (18)] and topoisomerase III [1I7D (17)] were superimposed using the backbone of comparable secondary structure elements and are shown from the same orientation. The ssDNA substrate is shown in orange. The insets show the structure of the entire enzyme; the active site and binding region is highlighted. The 2 nt at the 3′ end of the topoisomerase III DNA strand have been omitted for clarity.

found in the active site of *E.coli* topoisomerase I or other type IA topoisomerases have not been explored biochemically.

E.coli DNA topoisomerase III also belongs to the type IA family of DNA topoisomerases and has high degree of homology to *E.coli* topoisomerase I (15). When compared with *E.coli* topoisomerase I, it has a much weaker relaxation activity but a potent decatenating activity (16). The crystal structure of a complex formed by a mutant form (active site Tyr328 converted to Phe) of *E.coli* topoisomerase III and single-stranded DNA (ssDNA) has been determined (17); in addition, the structure of a different catalytically active mutant (H365R) form of the *E.coli* topoisomerase I 67 kDa transesterification domain bound to ssDNA has been reported (18) (Figure 1). In the topo III-DNA structure, Lys8 (topo III) has been found to be in a position to interact with the phosphate group of the scissile bond, so a conserved functional role was suggested for this residue. Examination of the sequence homology of bacterial and archeal topoisomerase I, as well as reverse gyrases showed that the N-terminal region between Leu5 and Lys13 is highly conserved (Figure 2). Besides the Glu9 residue previously determined to be important for DNA cleavage (9,10), a combination of a serine and a lysine at positions corresponding to Ser10 and Lys13 of *E.coli* topoisomerase I represent residues with side chains that could have potential catalytic functions. For bacterial topoisomerase III sequences, the conserved combination of lysine and serine corresponds to Lys8 and Ser10 of *E.coli* topoisomerase III. To examine the potential catalytic roles of the conserved lysine and serine found at the active site of type IA topoisomerases, site-directed mutagenesis was carried out to convert Ser10 and Lys13 of *E.coli* topoisomerase I to alanines, as well as Ser10 to Thr and Lys13 to Arg. The mutant enzymes were purified to homogeneity and characterized for the relaxation of negative supercoils, as well the ability to carry out each of the individual steps of interactions with DNA in the overall enzyme mechanism.

```
                    Glu9Ser10Lys13                  NCBI ID
EcTopA          MGKALVIVESPAKAKTINKYLGSDY           415338
HiTopA          MSKSLVIVESPAKAKTINKYLGSQY           1205601
AaTopA            MELFIVESPTKAKTIQKFLGKGF           6226245
TmTopA        MSKKVKKYIVVESPAKARTIKSILGNEY          881494
MgTopA          MIKNLVVIESPNKVRTLKQYLPSDE           1045802
SaTopA          MADNLVIVESPAKAKTIEKYLGKKY           14247020
RpTopA            MKLVIVESPAKAKTINKYLQDEF           6686044

SaRevG      ALQKVKTVLLVVESPNKARTISSFFSRPS           152943
MkRevG      TGRLARSALMIVESPNKARMIASLFSQRP           1173903
AaRevG      IKDLFKTTLVIVESPNKARTIAGFFGKPQ           7446038
TmRevG      VTKGGRSLLIIVESPTKAETLSRFLGRAS           2738604
AfRevG      EFDLIKPALFIVESPTKARQISRFFGKPS           7446075
SsRevG      VHFNISTGLLIVESPTKAKTIAKMFSRPS           7484129
ApRevG      GVELVRTALLVVESPNKARTIARFFGQPS           14601344

HiTopB            MRLFIAEKPSLARAIADVLPKPH           1204694
BsTopB          MSKTVVLAEKPSVGRDLARVLKCHK           2632726
SaTopB            MKSLILAEKPSVARDIADALQINQ           13702054
StTopB            MRLVLCEKPSQGRDIAKFLGATO           6513858
PmTopB            MRLFIAEKPSLARAIADVLPKPH           12720431
VcTopB          MTRLFIAEKPSLARAIADALPKPH           11387200
EcTopB            MRLFIAEKPSLARAIADVLPKPH           148026
                    Glu7Lys8Ser10
```

Figure 2. Alignment of type IA topoisomerase sequences in the region around Ser10 and Lys13 of *E.coli DNA* topoisomerase I. The bacterial and archeal type IA topoisomerase sequences are divided into three groups. Topoisomerase I (TopA), Reverse gyrase (RevG) and topoisomerase III (TopB) sequences are from Ec (*E.coli*), Hi (*Haemophilus influenza*), Aa (*Aquifex aeolicus*), Tm (*Thermatoga maritima*), Mg (*Mycoplasma genitalium*), Sa (*Staphylococcus aureus*), Rp (*Rickettsia prowazekii*), Mk (*Methanopyrus kandleri*), Af (*Archaeoglobus fulgidus*), Ss (*Sulfolobus shibatae*), Ap (*Aeropyrum pernix*), Bs (*Bacillus subtilis*), St (*Salmonella typhi*), Pm (*Pasteurella multocida*), Vc (*Vibrio cholerae*).

MATERIALS AND METHODS

Topoisomerase preparations

Wild-type recombisnant *E.coli* topoisomerase I was expressed and purified to >95% homogeneity by combination of phosphocellulose, hydroxylapitite and ssDNA agarose column

chromatography as described elsewhere (19). The topoisomerase I mutants were created with the QuikChange site-directed mutagenesis kit from Stratagene using plasmid pJW312 (20) as template. The sequence of the top strand oligonucleotides (custom synthesized by Genosys) for mutations at the underlined positions were 5′-CTTGTCATCGTTGAGCGCCCGGCAAAAG-3′ (S10A), 5′-GAGTCCCCGGCAGCAGCCAAAACGATC-3′ (K13A), 5′-CTTGTCATCGTTGAGACCCCGGCAAAAG-3′ (S10T), 5′-GAGTCCCCGGCACGAGCCAAAACGATC-3′ (K13R). Clones encoding the desired mutants were identified by DNA sequencing of the N-terminal region of the *topA* sequence on the plasmid. The mutant enzymes were expressed in *E.coli* AS17 (*topA*^{ts}) (20,21). Transformants were first grown to exponential phase at 30°C, before induction of the lacUV promoter in pJW312 by IPTG at 42°C (19,20). The mutant enzymes were purified with procedures similar to those used for the wild-type *E.coli* topoisomerase I. The final mutant enzyme preparations are >95% pure as determined by Coomassie blue staining of SDS gel after PAGE (data not shown).

Relaxation activity assay

Wild-type and mutant topoisomerases of the same concentration were diluted serially and assayed for relaxation activity in a standard reaction volume of 20 μl with 10 mM Tris–HCl, pH 8.0, 50 mM NaCl, 0.1 mg/ml gelatin, 6 mM $MgCl_2$ and 0.5 μg of supercoiled pJW312 plasmid DNA (purified by CsCl gradient centrifugation). After incubation at 37°C for 30 min., the reactions were stopped by adding 5 μl of 50 mM EDTA, 50% glycerol and 0.5%(v/v) bromophenol blue. The DNA was electrophoresed in a 0.8% (w/v) agarose gel with TAE buffer (40 mM Tris–acetate, pH 8.1 and 2 mM EDTA). The gel was stained with ethidium bromide and photographed over UV light.

Cleavage of 5′-labeled ssDNA

An oligonucleotide with phage λ DNA sequence 5′-CTCTGGCGGTGATAAATGGTT-3′ was labeled at the 5′ end with [γ-^{32}P]ATP and T4 polynucleotide kinase. It was then used as the forward primer in a PCR with λ DNA as template and a reverse oligonucleotide primer of the sequence 5′-CTCTTCCGCATAAACGCTT-3′, so that a 202 bp fragment was generated as PCR product by *Taq* DNA polymerase. Gel purification was carried out with the GenElute spin column (Sigma). After ethanol precipitation, this DNA fragment labeled on the 5′ end of one strand was resuspended in 10 mM Tris–HCl, pH 8.0 and 1 mM EDTA, denatured to single-strands and incubated with the wild type and mutant enzymes at 37°C for 10 min. After trapping the covalent complex and cleavage of DNA by alkaline treatment (22), the DNA was ethanol precipitated and analyzed by electrophoresis in an 8% sequencing gel. The 5′ end-labeled DNA cleavage products were visualized with the PhosphoImager Storm 760. The yield of the cleavage products was analyzed by the PhosphoImager software.

Gel mobility shift assay

The 39 base oligonucleotide 5′-GTTATGCAATGCGCTTTGGGCAAACCAAGAGAGCATAAC-3′ (PAGE purified from Genosys) with a strong topoisomerase I cleavage site (22) was labeled at the 5′ end with T4 polynucleotide kinase and [γ-^{32}P]ATP. The reaction mixture (10 μl) contained 20 mM Tris–HCl, pH 7.5, 100 μg/ml BSA, 12% glycerol, 1 pmol of the labeled 39mer and 0.8–8 pmol of wild type or mutant topoisomerase I. After incubation at 37°C for 5 min, the formation of gel mobility shift complex was measured by electrophoresis in a 6% polyacrylamide gel at 4°C with 0.5× Tris–borate–EDTA buffer and analyzed as described previously (10).

Oligonucleotide cleavage assay

The 5′ end-labeled oligonucleotide used in the gel mobility shift assay (5 pmol in 30 μl of 10 mM Tris–HCl, pH 8.0 and 1 mM EDTA) was incubated with the wild-type or mutant enzyme at 37°C. At different time points, 3 μl aliquots of the reaction mixture were mixed with equal volume of stop solution (79% formamide, 0.2 M NaOH and 0.04% bromophenol blue). The mixtures were heated at 80°C for 5 min before analysis by electrophoresis in a 15% sequencing gel. The fraction of cleaved oligonucleotide was determined by PhosphoImager Storm 760 analysis.

Limited Glu-C proteolytic digestion

Wild-type and mutant topoisomerase I proteins (15 μg) in 20 mM potassium phosphate, pH 7.5, 0.1 M KCl, 0.2 mM DTT were digested with sequencing grade Glu-C endoproteinase (from Roche Molecular Biochemicals) at 100:1 ratio at 37°C for the indicated length of time. The limited proteolysis was stopped by addition of equal volume of 2× gel loading buffer for the Laemmli SDS gel (23) and immersion in boiling water for 2 min. The digested samples were analyzed by electrophoresis in a 5–20% gradient SDS polyacrylamide gel followed by staining with Coomassie blue.

Molecular modeling

Models of the 'open' form of *E.coli* topoisomerase I complexed with ssDNA were constructed from crystallographic structures of the 'closed' form of *E.coli* topoisomerase I [1CY0] (13), the closed form of *E.coli* topoisomerase III complexed with ssDNA octamer [1I7D] (17), and the 'open' form of the isolated topoI domains II and III [1CYY] (24). The backbone atoms of alpha-helices in domains I, III and IV that are homologous between 1CYO and 1I7D were used to structurally position the ssDNA octamer in the model using Insight II (Accelrys). The ssDNA octamer (5′-CGCAACTT-3′) placed in the 1CY0 model was extended by 16 nt in a B-DNA conformation to form a 24mer (5′-CGCAACTTCATCAGTCTGCGCAGT-3′) since the octamer had been observed to be in a structure similar to B-DNA (17). The 'open' form of domains II and III was superimposed on the model using residues 218–225 and 468–472. Thus, the 'open' form model of topoisomerase I consists of 1CY0 residues 2–217 and 473–596, 1CYY residues 218–472, and a ssDNA based on the octamer from 1I7D. Four mutations (S10A, S10T, K13A, K13R) were introduced into the model of the wild-type enzyme using the Biopolymer module of Insight II, preserving the existing side chain dihedral angles.

The 'open' form models for the wild type and each mutant enzyme were transported into VMD (25) using the psfgen utility of NAMD (26). The solvate script of VMD was used

to place a cube of water around the 'open' form model stretching a minimum of 10 Å beyond the protein on all sides. A Poisson-Boltzmann calculation using APBS (27) with a coarse grid size of 225 × 193 × 257 with grid points located ~1.0 Å and a fine grid size of 112 × 96 × 128 with grid points located 0.5 Å was used to identify the location of electrostatic minima with water molecules around the 'open' form model. In order to generate electrostatically neutral simulation cells with an ionic strength of 150 mM, water molecules located at the electrostatic minima were replaced with 70 potassium, 4 sodium and 50 chloride ions such that all ions were at least 9 Å from each other; note that the K13A mutation had 71 potassium ions due to the replacement of a cationic residue with a neutral residue.

The CHARMM 27 force field (28,29) was used for all minimizations and molecular dynamic simulations. A cutoff of non-bonded and electrostatic interactions at 12 Å and switching between 10 and 12 Å was used. The simulation cells were minimized with NAMD in three steps. First, the residues immediately adjoining breaks formed from the construction of the 'open' form model were minimized for 1000 cycles without permitting any other atomic positions to move. Second, the water and ions were minimized for 100 000 cycles without permitting motion in the topoisomerase complex. In the third minimization of 100 000 cycles, the entire system was permitted to move.

The final minimized structures were used as the starting points for molecular dynamics simulations. Non-bonded interactions were computed using the same parameters as for energy minimizations. Electrostatic interactions were computed using the particle-mesh Ewald algorithm with a cubic spline, a tolerance of 10^{-6}, and a charge grid spacing of ~1.5 Å. Water geometries (using a TIP3P water model) were held rigid using the SHAKE algorithm. Each system was heated to 300 K over 60 ps using a time step of 1 fs; the initial heating phase was continued for another 10 ps for a total of 70 ps. Each system was equilibrated for 200 ps, and the production run was continued for an additional 2 ns. Data were collected at 5 ps intervals, and analyzed using VMD and the numerical computation package Octave (30).

Estimation of ionization and solvation energies. Estimates of the ionization energy due to solvation and electrostatic effects of the protonated forms of selected residues were made using the psfgen utility of NAMD (26) and APBS (27). In this procedure, the average structures of topoIA were modified using psfgen by replacing only one residue at a time with an altered form of the residue: either Asp111, Asp113 or Glu115. Four altered forms of the residues were prepared using slightly altered patches modeled on the CHARMM 27 force field topology files (28,29): two forms were protonated on either oxygen of the carboxylate to model protonated aspartates/glutamates, while two forms placed a neutral hydrogen on either carboxylate oxygen to model the charged aspartates/glutamates. These neutral hydrogens are used to maintain identical reentrant molecular surfaces between the protonated and charged forms of the affected residues and were modeled to avoid altering the electrostatic partial charges indicated for aspartate/glutamate. APBS was used to calculate a thermodynamic cycle linking topoisomerase protonated on one residue, topoisomerase with a neutral hydrogen on the same residue, and an isolated hydrogen located at the same position as the titrating proton. The Poisson–Boltzmann calculation using APBS used coarse grid sizes of 159 × 141 × 165 with grid points located ~0.72 Å and a fine grid size of 113 × 103 × 117 with grid points located ~0.51 Å, an ionic strength of 150 mM divided equally between cations/anions. Calculations were either performed in bulk solvent (with a dielectric of 78.54) or in vacuum (with a dielectric of 2) to estimate the solvation energy. The ionization energy for the *i*th residue [$E_I(i)$] is calculated as follows:

$$\begin{aligned} E_I(i) &= (E_{\text{topo1A}} + E_{\text{proton}}) - E_{\text{topo1AH}} \\ &= (E_i^{\text{Topo1Asolvent}} - E_i^{\text{Topo1Avacuum}}) \\ &\quad + (E^{\text{Protonsolvent}} - E^{\text{Protonvacuum}}) \\ &\quad - (E_{iH}^{\text{Topo1Asolvent}} - E_{iH}^{\text{Topo1Avacuum}}). \end{aligned}$$

Energies calculated for either form of a protonated aspartate or glutamate were averaged. This protocol has been demonstrated to reproduce the standard ionization energy test case of the mono-carboxylate acetic acid within an error of 0.7%.

RESULTS

Mutations in Ser10 and Lys13 result in reduction of DNA relaxation activity

To investigate the potential catalytic role of the serine and lysine residue conserved in the active site region of bacterial topoisomerase I, Ser10 and Lys13 of *E.coli* DNA topoisomerase I were mutated to alanines. The resulting mutant enzymes were expressed and purified to near homogeneity for biochemical characterization. Assays using negatively supercoiled plasmid as substrate demonstrated that the resulting S10A mutant enzyme had 5- to 10-fold and K13A mutant enzyme had around 50- to 100-fold reduction in relaxation activity under the standard assay conditions (Figure 3A). To determine if changing Ser10 to a threonine residue, which also has a hydroxyl group in the side chain, and changing Lys13 to another basic amino acid arginine allowed retention of activity, mutants S10T and K13R were constructed and purified. Relaxation activity assays showed that introduction of a different side chain with similar functionality but different steric properties at these two positions resulted in even lower relaxation activity for the enzyme (Figure 3B). The *in vivo* activity of these mutant enzymes was measured by their ability to complement the *topA* mutation in strain AS17 for growth at the non-permissive temperature of 42°C (20,21). The results (Table 1) showed that mutations at Ser10 and Lys13 greatly reduced the ability of topoisomerase I to support growth of the *E.coli* cells, as expected from the loss of relaxation activity.

The S10A and K13A mutants were not affected in non-covalent DNA binding

The first step in relaxation of negatively supercoiled DNA is the non-covalent binding of DNA with a single-strand region. The formation of a gel mobility shift complex with a 5′ labeled oligonucleotide was assayed for the wild-type and mutant enzymes. This oligonucleotide had a strong topoisomerase I cleavage site (22) and was designed to form a stem–loop

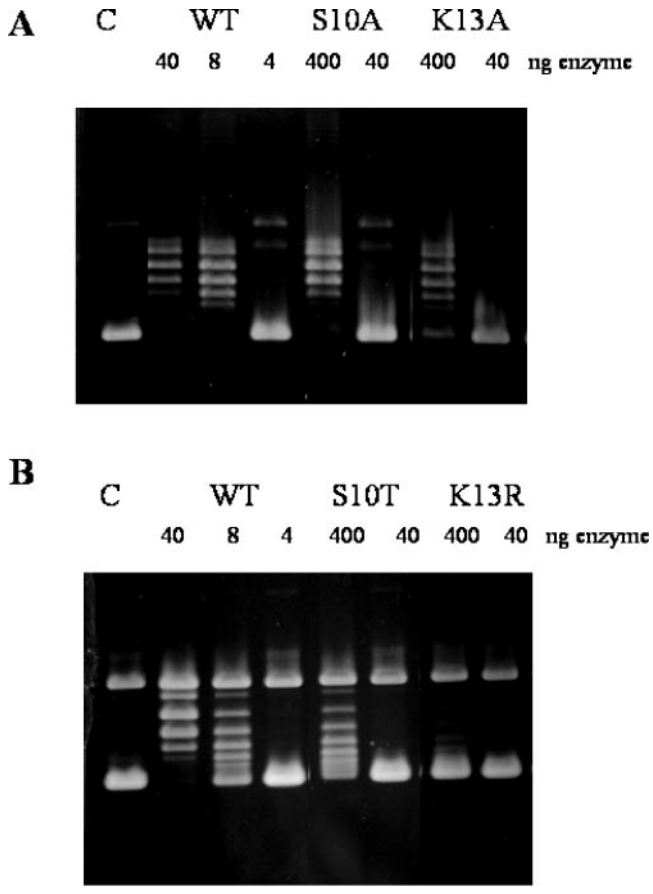

Figure 3. Comparison of the relaxation activity of wild-type topoisomerase I and mutant enzymes with substitutions at Ser10 and Lys13. (**A**) Serial dilution of the WT (wild-type) and S10A and K13A topoisomerase I. (**B**) Serial dilution of the WT (wild-type) and S10T and K13R topoisomerase I. C, control with no enzyme added.

Table 1. Test of *in vivo* complementation by the plasmid encoded topoisomerase I mutants

Plasmid encoded topoisomerase I	*In vivo* complementation
Wild-type	1.0
S10A	10^{-3}
K13A	10^{-4}
S10T	10^{-4}
K13R	10^{-4}
None	$<10^{-4}$

Plasmid pJW312 encoding either wild type or mutant topoisomerase I was transformed into AS17 containing a pMK16*lacIq* plasmid (20). Serial dilutions of cultures of the transformants (grown overnight at 30°C) were plated on Luria–Bertani plates with ampicillin and incubated at both 42 and 30°C. After 18–36 h incubation, the ratio of viable colonies obtained at 42°C versus 30°C is determined.

structure (Figure 4) to place the cleavage site at the junction of ssDNA and double-stranded DNA so binding of the oligonucleotide at the enzyme active site should be favored. The structure of the substrate allowed the 5′ end label to stay bound in the enzyme complex under the non-denaturing gel condition even if the initial complex has been converted to a cleaved complex. Therefore the gel shift complex can be

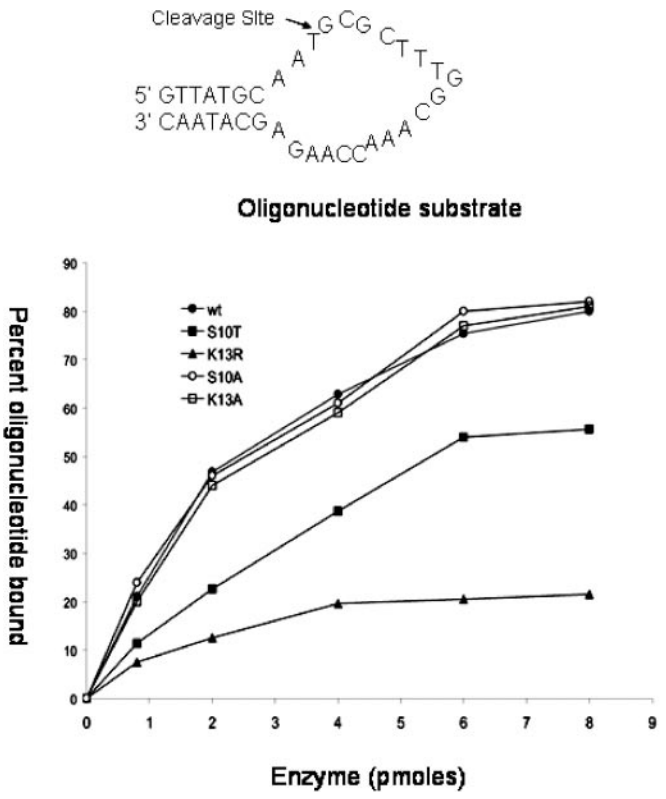

Figure 4. Effect of the mutations on the formation of the initial non-covalent complex as assayed by the gel mobility shift assay using a 5′ end-labeled oligonucleotide.

evaluated as representative of the initial non-covalent complex. The fraction of the initial complex converted to cleaved complex was quantified separately by denaturing gel as described below. The results of the gel mobility shift assay (Figure 4) showed that the S10A and K13A mutants had DNA binding affinity similar to that of the wild-type enzyme, while the S10T and K13R mutants had reduced DNA binding affinity. A lower amount of oligonucleotide–enzyme complex was seen at saturation for the S10T and K13R mutants. The non-covalent complexes formed by these two mutants may be significantly less stable during gel electrophoresis when compared to the complexes formed by the wild-type and S10A and K13A mutant enzymes. The results of the S10A and K13A mutants showed that the loss of side chain functions at Ser10 and Lys13 affected the relaxation activity after initial binding of the DNA substrate, because these two mutants were normal in the formation of non-covalent complex with DNA.

The side chains of Ser10 and Lys13 are required for DNA cleavage activity

The ability of the mutant enzymes to cleave a single-strand of DNA was compared with that of the wild-type enzyme using 5′-labeled ssDNA of 202 bases in length. The transient cleaved complex represents a smaller percentage of the enzyme–DNA complex and can be trapped by the addition of alkaline to denature the enzyme (31). Quantification of the results (Figure 5) showed that the amount of transient DNA cleavage products trapped for these mutant enzymes were 6% or less of

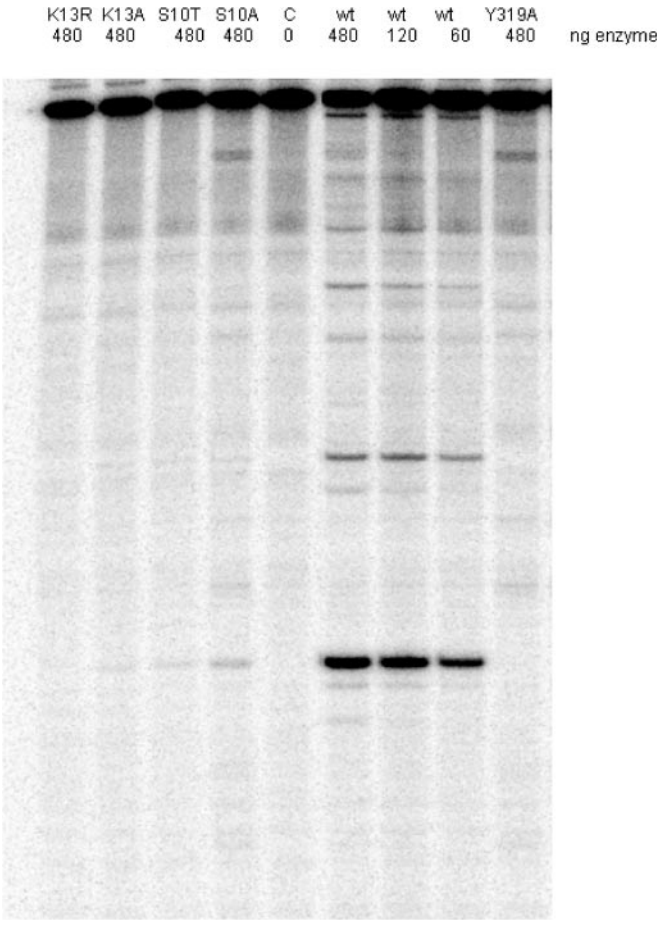

Figure 5. DNA cleavage activity of the wild-type and mutant enzymes. ssDNA labeled at the 5′ end was used as substrate for analysis of the cleavage activity using 400 ng of WT (wild-type) and mutant enzymes. C, control with no enzyme added.

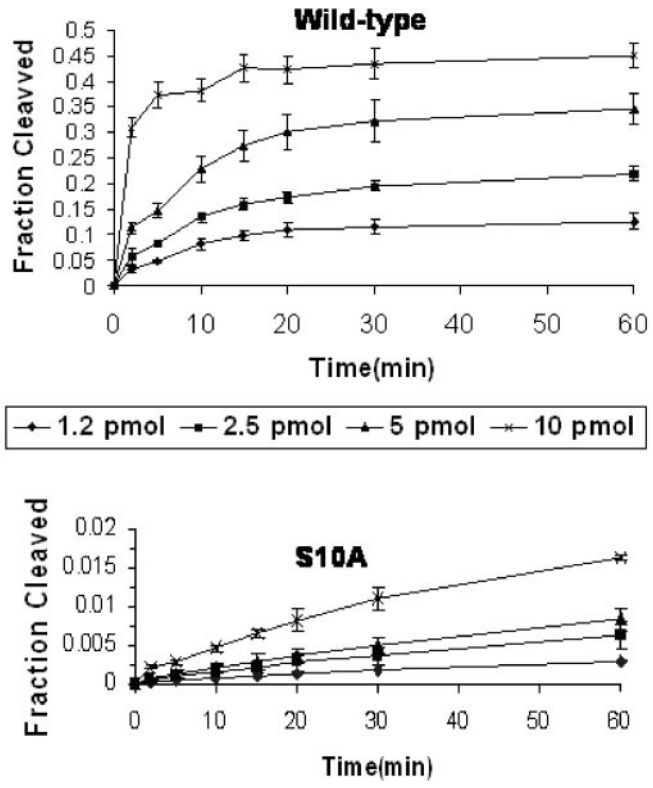

Figure 6. Time course of oligonucleotide cleavage by wild-type and S10A mutant topoisomerases at different enzyme:substrate ratios. Each reaction contained 5 pmol of 5′-labeled oligonucleotide substrate. Results are from the average of three experiments.

that of the wild-type enzyme. The reduction in formation of cleaved DNA complex which precedes DNA strand passage in the enzyme mechanism would account for the loss of relaxation activity for these mutants.

The cleavage activity of the S10A mutant was also assessed with the same oligonucleotide substrate used in the non-covalent DNA-binding assay. After alkaline treatment and under denaturing gel electrophoresis conditions, the cleaved DNA with the 5′ end-labeled dissociated from the covalent enzyme-DNA adduct and was quantified as the fraction of input DNA converted into the reduced size fragment. With the wild-type topoisomerase I, the maximal yield of cleaved DNA was reached before 20 min of the incubation for all the enzyme:substrate ratios tested. The maximal yield of cleaved complex at each enzyme:substrate ratio tested correlates with the amount of enzyme present since for each cleaved DNA molecule formed, one enzyme molecule was covalently bound to the other half of the input substrate (Figure 6). With the S10A enzyme, the yield of the cleaved complex observed was ~30-fold lower than the wild-type enzyme at each enzyme: substrate ratio even after 60 min of incubation. This is consistent with the interactions between the enzyme and the substrate at the active site being affected by the mutation, resulting in reduction of the cleavage activity, even though the initial complex was formed at the same level as the wild-type enzyme. The rates of cleavage by the other mutants were too low to be analyzed.

The S10T and K13R mutants do not have severe changes in protein folding

The S10T and K13R mutants were found to have reduced non-covalent DNA-binding affinities that could be due to defects in protein folding arising from the introduction of the more bulky side chains by the mutations. To determine if these two mutants had severe changes in protein folding compared with the wild-type topoisomerase I, limited proteolysis was carried out for different lengths of time with Glu-C endoproteinase and the products were analyzed by SDS–PAGE. The results (Figure 7) showed that these two mutants had the same protease digestion products profile as the wild-type topoisomerase I. Therefore it is unlikely that these mutations have caused severe changes in the folding of the enzyme molecule.

Molecular modeling of the active site of *E.coli* DNA topoisomerase I

The molecular dynamics simulations do not capture large-scale deviations in either domain 1 or 4 that alter the topoisomerase I conformation from the crystal structure: the average structures of domain 1 and the 8 nt bound to this domain remain within an root mean square deviation

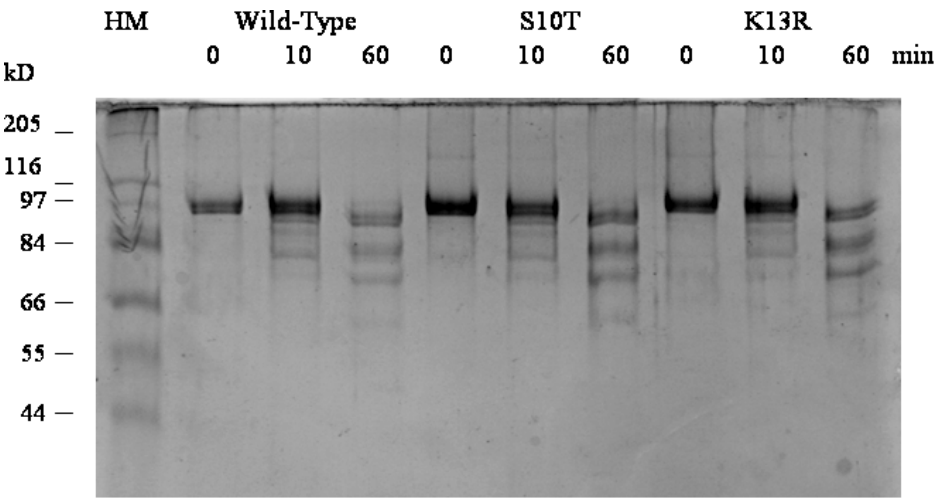

Figure 7. Limited proteolysis by Glu-C endoproteinase. The time course of digestion of wild-type topoisomerase I by Glu-C endoproteinase is compared with the S10T and K13R mutant enzymes.

(r.m.s.d.) of 1.8 Å, while the average structures of domains 1, 4 and the nucleotides remain within an r.m.s.d. of 2.8 Å (data not shown).

The observed large-scale motion in domains 2 and 3 in the mutated enzymes may drive the increasing r.m.s.d. observed in domain 4, owing to the connections and proximity of these domains. However, the limited scale of the 2 ns simulations does not allow us to sample a sufficiently large ensemble to make a statistically significant determination of correlated motions in the topoisomerase domains. In the wild-type simulation, we note that these motions initiate closing of the open form complex by bringing domains 1 and 3 closer by ~10 Å (data not shown). Helix O (residues 496–507) also moves to clamp down over the DNA in the complex (Figure 8); the motion of this helix appears to occur as a result of DNA occupancy of the active site and the closing motion of the WT enzyme, as suggested by Perry and Mondragón (18). We note that the enzyme closes rapidly during the simulations, with the distance between domains 1 and 3 closing by 20 Å within 10 ns (data not shown).

In the wild-type complex, Lys13 interacts with Glu9 and Asp111, mirroring the interactions observed in the closed co-crystal complexes (17,18); however the Lys13 NZ group more closely follows the geometry observed in the closed enzyme without DNA (13) and is ~7 Å from the scissile phosphate (Table 2 and Figure 9D). Ser10 forms a direct hydrogen bond with phosphate 8, adjacent to the scissile nucleotide at position 7 (Figure 9A). This interaction between Ser10 and the DNA is slightly different from the crystal structure of the topo III closed complex (17), where this residue makes an analogous water-mediated contact to the terminal phosphate of the octamer. These differences may be due to the difference between the 'open' and 'closed' conformations of the enzyme, or the presence of 16 additional nucleotides beyond the crystallographic octamer.

The two mutations of Ser10 have different effects on the active site structure. In the S10A topoisomerase I mutant, Ala10 is unable to form a hydrogen bond with phosphate 8 (Figure 9B). This absence of this interaction increases the flexibility of Ala10 and Lys13, perturbing the

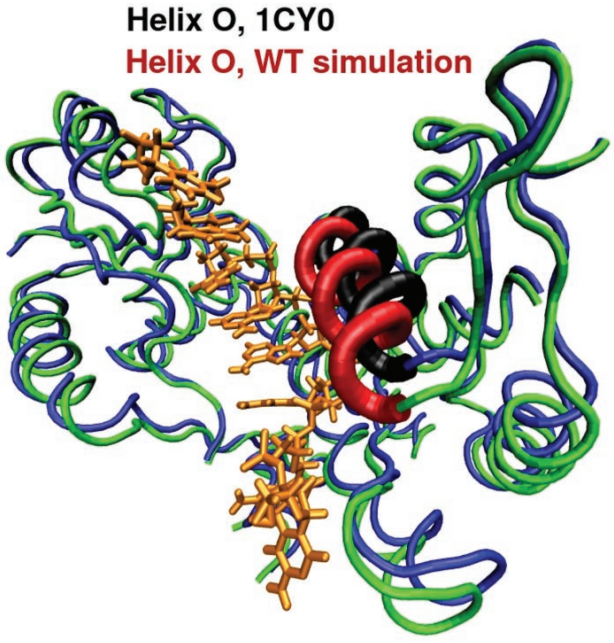

Figure 8. Movement of helix O in the WT complex. The crystal structure of *E.coli* topoisomerase I [1CY0, (13)] is shown in blue; helix O of 1CYO is shown in black. The average structure of the wild-type topoisomerase I from the final 1.34 ns of the simulation is shown in green; helix O of the wild-type enzyme is shown in red. The ssDNA substrate in the wild-type simulation is shown in orange.

interactions between Lys13, Asp111 and the scissile phosphate (Table 2).

Intriguingly, the loss of the hydroxyl interaction with phosphate 8 results in a small rotation of the phosphate 8 group; the rotation is towards the neutral alanine side chain, presumably due to the attractive forces of the nearby backbone nitrogens and the K13 side chain. This rotation may force the 7 deoxyribose (adjacent to the scissile phosphate) to move rigidly without altering the deoxyribose's conformation (Table 3), possibly due to the surface constraints underneath the ribose provided by Glu9, Val31 and Gly32.

Table 2. Interaction distances of residues 10 and 13 in wild-type and mutant topoisomerases

Mutant	S10:OG-8:O1P	S10:CB-K13:CB	K13:NZ-E9:OE1/2	K13:NZ-D111:OD1/2	K13:NZ-Thy7:P
WT	2.7 ± 0.2	3.7 ± 0.2	2.8 ± 0.2	3.1 ± 0.3	6.9 ± 0.4
S10A	3.6 ± 0.2*	4.2 ± 0.5	2.7 ± 0.1	4.6 ± 1.1	8.5 ± 1.0
S10T	3.8 ± 0.2	5.0 ± 0.2	2.7 ± 0.2	3.2 ± 0.5	7.3 ± 0.5
K13A	2.7 ± 0.4	4.7 ± 1.0	6.2 ± 0.9*	6.8 ± 0.7*	10.1 ± 0.8*
K13R	2.7 ± 0.2	4.0 ± 0.3	3.9 ± 0.2*	5.9 ± 1.3*	9.7 ± 1.1*

Interaction distances are given in angstroms as the mean over 400 structures sampled at a frequency of 5 ps; the SD of each distance is indicated. For residues Glu-9, the reported distance is the average of the two distances measured between residue 13 and Glu9:OE1 and between residue 13 and Glu9:OE2; similarly, the computed distances for Asp111 are also the average of two distances. For the three mutants S10A, K13A and K13R, certain interactions (indicated by asterisks) could not be calculated due to atoms not present in the structures; in each case, alternative atoms were chosen. For the S10A mutant, the atom CB was substituted for OG. For the K13A mutant, the atom CB was substituted for NZ. For the K13R mutant, the atoms NH1 and NH2 were substituted for NZ.

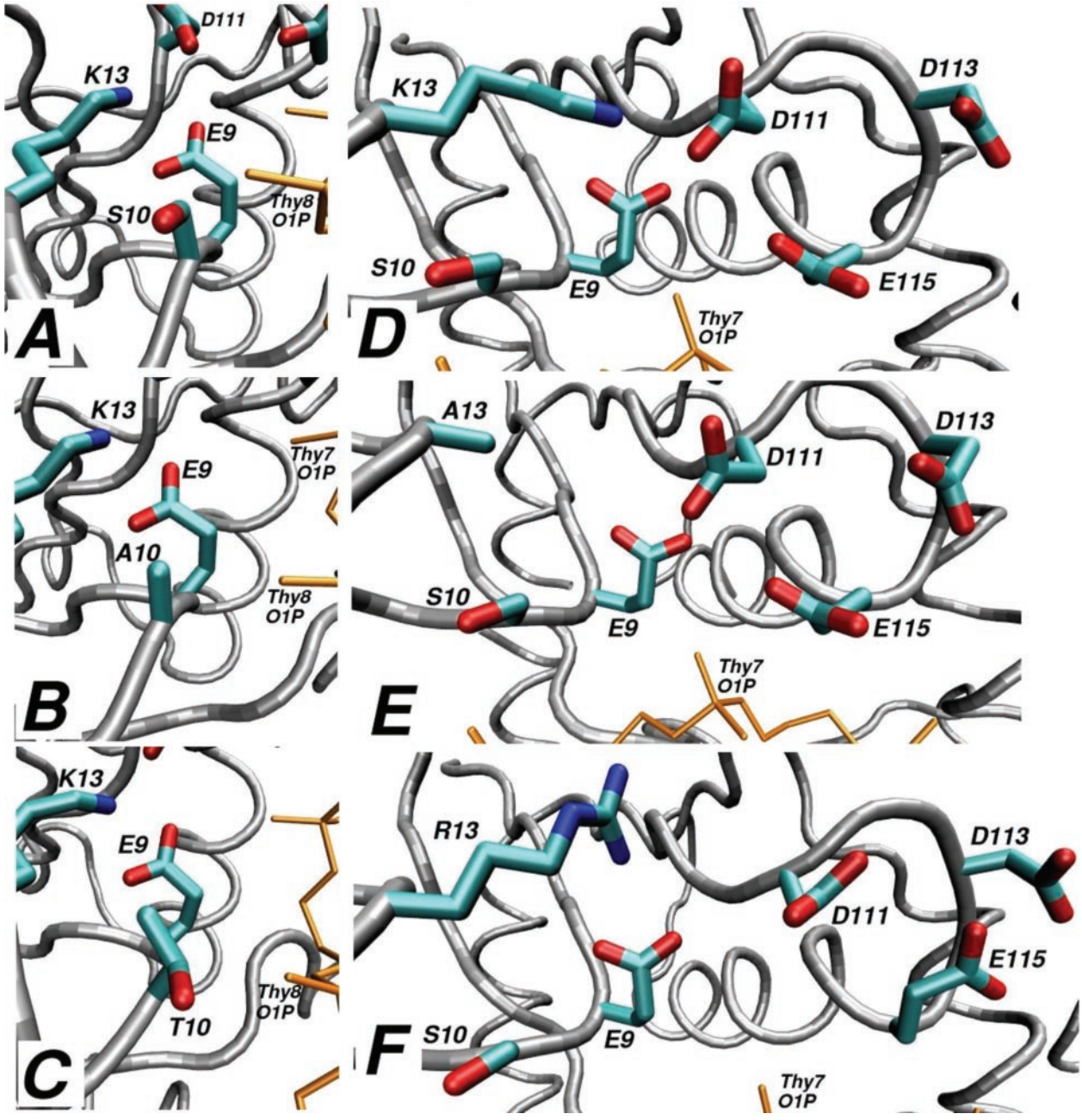

Figure 9. Effects of mutations on simulated models of topoisomerase I. (A–C) Mutations of S10. (D–F) Mutations of K13. (**A**) wild-type enzyme. (**B**) S10A mutant enzyme. (**C**) S10T mutant enzyme. (**D**) Wild-type enzyme.(**E**) K13A mutant enzyme. (**F**) K13R mutant enzyme. Each structure is a minimized average structure from approximately the final 1.2 ns of each simulation, superimposed using the backbone atoms of domains I and IV.

In turn, the rigid motion of the 7 deoxyribose may transmit a larger force to the scissile phosphate and the 6 deoxyribose. The zeta backbone dihedral angle just past the scissile phosphate (running from 7:O5′–7:P–6:O3′–6 C3′) changes from a −60-synclinal conformation in the WT to a −130-antiplanar conformation in the S10A mutant. The rotation of this backbone dihedral alters the deoxyribose conformation of residues 6 and 5, forcing them from a c3′-endo 'northern' pucker to a c2′-endo 'southern' pucker conformation. These altered sugar conformations have two effects: the remaining path of the DNA substrate (towards deoxyribose 1) rotates to follow the riboses and the 6 deoxyribose sterically clashes with Glu115 (Figure 10). In the wild-type enzyme, the C3′ atom of the 6 deoxyribose is 6.3 Å from Glu115 CB, but this has shortened to 3.9 Å in the S10A mutant. Owing to the steric clash, Glu115 rotates towards Asp113 and Asp111, altering the conformation of the catalytic triad observed in the enzymes that retain a hydroxyl at residue 10.

Table 3. Deoxyribose conformations in WT and S10A complexes

Deoxyribose	WT		S10A	
Thy 8	160.0	c2′ endo	160.8	c2′ endo
Thy 7	16.0	c3′ endo	20.0	c3′ endo
Cyt 6	9.5	c3′ endo	145.3	c1′ exo c2′ endo
Ade 5	15.8	c3′ endo	170.4	c2′ endo
Ade 4	155.1	c2′ endo	166.0	c2′ endo

Pseudorotation phase angles (in units of degrees) are sampled from the average structure from approximately the last 1 ns of the simulation.

The combined effect of this novel conformation of the catalytic triad enhances the local electrostatics (Figure 11A) and may interfere with magnesium binding. We note that isolated carboxylates possess pK_a's that typically range near 4.1, but the close proximity of the carboxylates of the catalytic triad in the S10A mutant is expected to substantially raise one or more pK_a values (owing to collective influence of the individual anion's electrostatic field). When the pH dependence of the S10A mutant was compared with that of the wild-type topoisomerase (Figure 11B), it was observed that while the wild-type enzyme was active at pH 5.5, the S10A mutant required pH to be elevated to 6.0 for relaxation activity to be observed, suggesting a protonation event between pH 5.5–6.0 in the S10A mutant to influence the activity. Calculations of the solvation and electrostatic energies stabilizing the protonated forms of Asp111 and Asp113 in the S10A enzyme show that both residues are

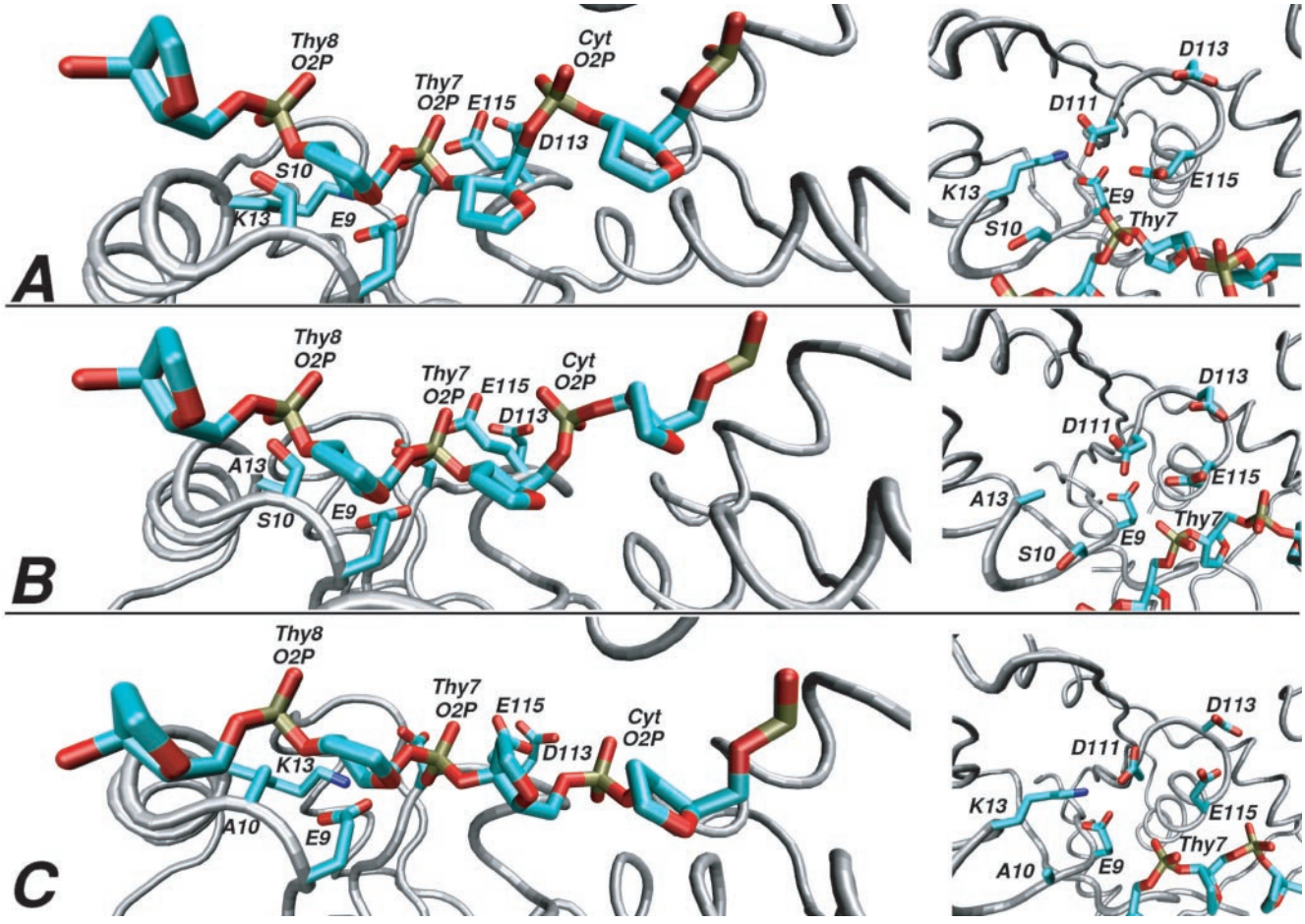

Figure 10. Conformational changes due to loss of the S10 hydroxyl. (**A**) Wild-type enzyme. (**B**) K13A mutant enzyme. (**C**) S10A mutant enzyme. Left, side views, illustrating the conformational changes in the DNA substrate backbone. Bases have been omitted for clarity. Right, top view, looking down on the acidic residues in the active site. Each structure is a minimized average structure from approximately the final 1.2 ns of each simulation, superimposed using the backbone atoms of domains I and IV.

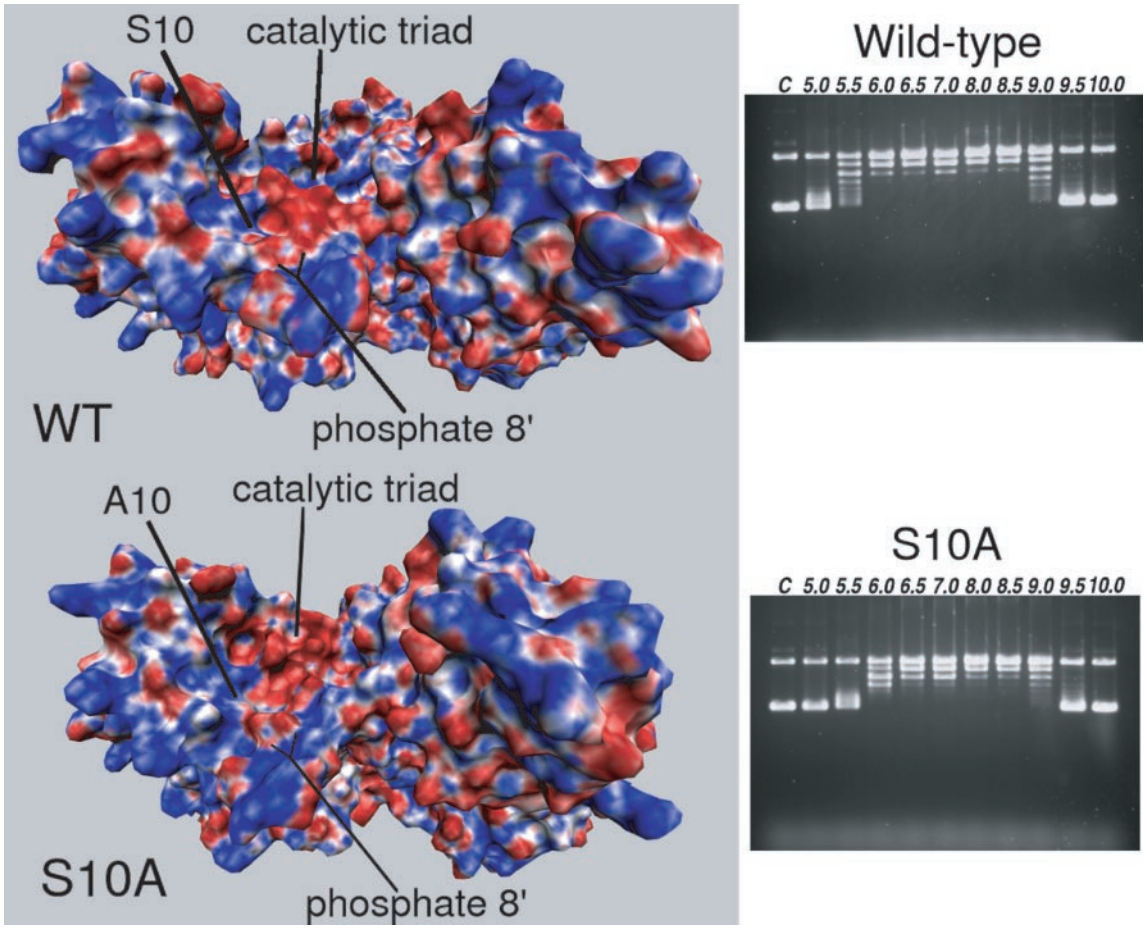

Figure 11. Surface potential map and alteration of pH profile for wild-type and S10A mutant topoisomerases. (**A**) Top left, wild-type enzyme. Bottom left, S10A mutant. The electrostatic potential, mapped on the molecular surface constructed using MSMS (38), was computed using APBS (27) to focus on the active site with a final grid spacing of ~0.5 Å. Each structure is a minimized average structure from approximately the final 1.2 ns of each simulation, superimposed using the backbone atoms of domains I and IV. (**B**) The effect of reaction pH on the relaxation activity of wild-type (top right) and S10A mutant (bottom right) enzymes. The reaction pH was maintained with 36 mM Mes for pH 5.0–6.5, Tris for pH 7.0–8.5, Ches for pH 9.0–10.0. The enzyme (400 ng) was first equilibrated with buffer of the indicated pH before addition of supercoiled plasmid DNA and 8 mM $MgCl_2$. The final reaction mixture (13 µl total volume) was incubated at 37°C for 30 min. C, control with no enzyme added.

more stable in this conformation as neutral protonated aspartates than in the wild-type enzyme. The protonated form of Asp111 in the S10A mutant is stabilized by an average energy difference of −8.9 kJ/mol over the protonated Asp111 in the wild-type enzyme, corresponding closely to a pK_a increase of ~1.55 U. Compared with the model compound of an isolated carboxylate with a pK_a near 4.1, this raises the pK_a predicted of Asp111 in the S10A enzyme to ~5.7 (neglecting energies due to conformational adjustments). We note that the Asp111 is an invariant residue in TOPRIM domains and is expected to participate in magnesium binding; protonation of this residue would interfere with the magnesium ion and DNA cleavage. The close correspondence between the computed DNA conformations and novel catalytic triad conformation and the experimental pH shift of the S10A enzyme strongly suggests the validity of the structures sampled during the computational simulations. The residual activity that remains in the S10A mutant (Table 1) also suggests that a minor subset of conformations may exist in which the DNA substrate resembles the wild-type complex; however, such structures corresponding to active (i.e. wild-type) forms were not observed in this limited modeling of the S10A mutant and may be observed during longer duration simulations.

In the S10T mutant, Thr10 forms a hydrogen bond with phosphate 8 (Figure 9C); however, this interaction is longer than the Ser10 interaction, indicating its relative weakness. The CG2 methyl group of Thr10 pushes against the alkyl side chain of Lys13; thus, Thr10 also increases the distance between Thy8 and Lys13 and increases the motion of Lys13 relative to the wild-type complex (Table 2). This collision between Thr10 and Lys13 also forces Thr10 to move away from the clash; however, Glu9 is adjacent to Thr10 and also moves backwards. In the wild-type complex, the distance between the Glu9 CD and the Asp113 CG is 10.7 Å; in the S10T mutant, this distance increases to 11.7 Å. The increase of this distance suggests that the S10T mutation may force Glu9 into a geometry where it may be unable to interact within the catalytic triad and the magnesium ion possibly coordinated at this site.

Although Ala13 in the K13A mutant is unable to make interactions with the acidic residues of the active site, no other distortions occur to the residues Glu9, Asp111, Asp113 and Glu115 (Figure 9E). The decreased activity

following the loss of the lysine side chain suggests that Lys13 may play a role in the catalytic site, perhaps as a polarizing influence on Glu9. However, additional investigation of the active site is required to evaluate this hypothesis.

The Arg13 residue in the K13R topoisomerase I mutant is a larger residue than lysine, and is unable to fit in the space assigned to Lys13 and accommodate the interactions with both Glu9 and Asp111. Arg13 continues to interact with Glu9, owing to the favorable electrostatics but these interactions become distorted due to the size of Arg13 (Figure 9F). Arg13's guanidinium moiety pushes against Glu9, altering the conformation of Glu9. Asp111 rotates out of the acidic pocket due to Glu9's motion, and Asp111's motion pushes Glu115 and Asp113; in essence, Arg13's intrusion into the acidic pocket forces a 'domino effect' where all the acidic residues shift their conformation. Glu9 also pushes on the Arg13 guanidinium group, forcing the Arg13 backbone to move away by ~1 Å. This motion shifts the entire backbone in this region (including Ser10) by ~1 Å; in turn, the path of the ssDNA shifts to follow these interactions. The distorted active site of the K13R mutant is apparently catalytically incompetent due to the severe steric clashes.

DISCUSSION

The multi-step process of change of linking number catalyzed by topoisomerases is likely to require participation of different functional groups in different steps of the reaction. In the current mechanism of *E.coli* topoisomerase I, Tyr319 is responsible for nucleophilic attack on DNA and formation of the covalent bond between the enzyme and the 5′ phosphate of the cleaved DNA (7). Glu9 found also in the active site has been implicated in the process of DNA cleavage (9,10). In its proximity, Ser10 and Lys13 are conserved residues with side chains that could also participate in the catalytic process. Results presented here on the site-directed mutants support a role for these two residues in the DNA cleavage step of the enzyme mechanism. Altering these residues to alanines did not affect non-covalent binding to DNA, but significantly reduced the formation of the cleaved DNA complex. The changes of Ser10 to Thr and Lys13 to Arg had more severe effects on the enzyme, reducing also the non-covalent binding of enzyme to DNA. Although proteolytic digestion of the S10T and K13R mutants did not indicate severe defects in protein folding, the changes in the side chains in these substitutions could potentially affect the structure of the junction region between domains I and III at the active site, affecting also the non-covalent interaction of the enzyme with the single-strand of DNA that has to be positioned at the active site for cleavage.

In the crystal structure of *E.coli* topoisomerase III complexed with ssDNA (17), the lysine residue (Lys8) that corresponds to Lys13 in topoisomerase I is in a position to interact with the phosphate group of the scissile bond (Figure 1). The importance of this residue in DNA cleavage as suggested by the structural data (17) is now demonstrated biochemically in this study.

In the structure of the 67 kDa N-terminal fragment of topoisomerase I, the side chains of both Ser10 and Lys13 are in the vicinity of Tyr319 with their relative positions switched when compared with Lys8 and Ser10 of topoisomerase III (Figure 1). The positively charged side chain of Lys13 is expected to interact with either the scissile phosphate and/or the acidic pocket of Glu9/Asp111/Asp113 via electrostatic interactions. The results from our molecular modeling simulations support the interaction of Lys13 with the acidic pocket, particularly with Glu9 and Asp111. Although our models show that the distance from Lys13's amide group to the scissile phosphate is ~7 Å, conformational changes in the enzyme might easily halve the distance between these groups. Modeling studies currently underway simulating the transition of the 'open' complex to the 'closed' complex may reveal further details of these proposed interactions.

In the crystal structure of the topoisomerase III–DNA complex (17), the side chain of Ser10 does not appear to be in a position to participate directly in DNA cleavage. Nevertheless, this residue is in proximity to the phosphate immediately 3′ of the scissile phosphate and a water-mediated hydrogen bond is observed between Ser10 and this phosphate. The topoisomerase enzyme used in the crystallization of this complex has phenylalanine substituted for the active site tyrosine. It is also in the absence of the Mg^{2+} ions required for catalytic activity and using a short oligonucleotide substrate. It cannot be ruled out that with the conformational changes expected from topoisomerase in the presence of either an active site tyrosine, Mg^{2+} ions, or with longer ssDNA substrates that the position of the side chain of this serine residue could change to participate more directly in DNA cleavage. In our simulated topoisomerase I complex with a longer oligonucleotide, the side chain of Ser10 forms a hydrogen bond directly with the phosphate 3′-adjacent to the scissile phosphate. This interaction appears to be crucial to the positioning of the DNA substrate in the active site; when this hydroxyl was removed in the S10A mutant, deoxyribose 6 located 5′ to the scissile phosphate shifted from a 'northern' pucker to the 'southern' pucker typical of B-form DNA. In the F328Y topo-III and H365R topo-I cocrystals (17,18), the analogous deoxyriboses are also observed in a 'northern' pucker conformation. The 'northern' ribose conformations uniquely position O3′ along the equitorial plane of the ribose which orients the adjacent phosphate oxygens towards the tyrosine nucleophile. Thus, Ser-10 aides the positioning of the scissile phosphate for DNA cleavage and may account for the conserved presence of this serine residue among type IA topoisomerase sequences. We propose that helix O and Ser10, respectively are the 5′ and 3′ ends of a clamp that holds the DNA substrate in the active site properly positioned for cleavage.

Topoisomerase mechanisms share a common feature with some enzymatic phosphoryl transfer reactions in the formation of a covalent intermediate. In these two-stage mechanisms, an enzyme nucleophile first attacks a phosphorus to form a stable covalent intermediate. In the second stage of the reaction, the covalent intermediate is in turn attacked by a nucleophile to generate the free enzyme again and reaction products (32). Enzymatic phosphoryl or nucleotidyl transfer reactions are often facilitated by surrounding the attacked phosphate with positively charged groups including the side chain of lysine residues (33,34). In the study of the mechanism of enzymatic phosphoryl transfer by phosphoserine phosphatase, a hydrogen bond between an active site serine residue and a non-bridging oxygen of the phosphoryl group, as well as salt bridge interactions by an active site lysine residue,

have been proposed to be important for ground-state stabilization (32,35). Therefore examples of utilization of a combination of conserved active site serine and lysine residues to catalyze the formation of a phosphoryl-enzyme covalent intermediate are already known.

A role for the conserved Arg321 with its positively charged guanidinium group close to the active site tyrosine hydroxyl in promoting nucleophilic attack by Tyr319 by stabilization of the negatively charged phenolate ion has been proposed for the mechanism of *E.coli* DNA topoisomerase I (9,13,24). The corresponding arginine Arg330 in *E.coli* DNA topoisomerase III was observed to contact the scissile phosphate in the complex with ssDNA (17). A similarly positioned arginine residue may have similar functions in type II topoisomerases (36,37). Based on the structure of *E.coli* DNA topoisomerase III complexed to ssDNA, it was also proposed that Glu7 of topoisomerase III (corresponding to Glu9 of *E.coli* DNA topoisomerase I) acts as a general acid catalyst by donating a proton to the leaving 3′-oxygen atom of the scissile bond during DNA cleavage and may also act to abstract a proton from the free 3′-hydroxyl group during nucleophilic activation for DNA religation (17). Mutagenesis studies of His365 of *E.coli* DNA topoisomerase I led to the proposal that His365 donates a proton to Asp111 which then relays the charge to Glu9 for its protonation (14). The stable salt bridge that Lys13 forms with Glu9 and the observed activity defects in alanine mutagenesis suggests that Lys13 may participate in the proton transfer.

This study provides biochemical evidence that contact with the 3′-downstream phosphate involving Ser10 may also be important for the cleavage step of catalysis and that a second positively charged side chain may be used in the active site to donate a proton and/or contact the scissile phosphate. Similar roles have also been suggested for other active site residues (9,10,18). Active site residues in the topoisomerase may play multiple roles, further underscoring the finding that few alanine mutations completely eliminate relaxation activity (9).

Additional structural information on the different conformations of the enzyme and its complex with DNA, molecular modeling of the different topoisomerase states and the proposed catalytic mechanisms, and mutagenesis data on other conserved amino acids with potential catalytic roles will help elucidate the mechanism of this class of enzyme.

ACKNOWLEDGEMENTS

We thank Dr James C. Wang for helpful discussions. This research was supported by a grant (GM54226) from the National Institutes of Health. NAMD was developed by the Theoretical and Computational Biophysics Group in the Beckman Institute for Advanced Science and Technology at the University of Illinois at Urbana-Champaign. Funding to pay the Open Access publication charges for this article was provided by NIH grant GM54226.

Conflict of interest statement. None declared.

REFERENCES

1. Champoux,J.J. (2001) DNA topoisomerases: structure, function, and mechanism. *Annu. Rev. Biochem.*, **70**, 369–413.
2. Tse-Dinh,Y.-C. (1998) Bacterial and archeal type I topoisomerases. *Biochim. Biophys. Acta*, **1400**, 19–27.
3. Drlica,K. (1992) Control of bacterial DNA supercoiling. *Mol. Microbiol.*, **6**, 425–433.
4. Luttinger,A. (1995) The twisted 'life' of DNA in the cell: bacterial topoisomerases. *Mol. Microbiol.*, **15**, 601–606.
5. Masse,E. and Drolet,M. (1999) *Escherichia coli* DNA topoisomerase I inhibits R-loop formation by relaxing transcription-induced negative supercoiling. *J. Biol. Chem.*, **274**, 16659–16664.
6. Tse-Dinh,Y.-C. and Wang,J.C. (1986) Complete nucleotide sequence of the *topA* gene encoding *Escherichia coli* DNA topoisomerase I. *J. Mol. Biol.*, **191**, 321–331.
7. Lynn,R.M. and Wang,J.C. (1989) Peptide sequencing and site-directed mutagenesis identify tyrosine-319 as the active site tyrosine of *Escherichia coli* DNA topoisomerase I. *Proteins*, **6**, 231–239.
8. Lima,C.D., Wang,J.C. and Mondragón,A. (1994) Three-dimensional structure of the 67K N-terminal fragment of *E. coli* DNA topoisomerase I. *Nature*, **367**, 138–146.
9. Chen,S.-J. and Wang,J.C. (1998) Identification of active site residues in *Escherichia coli* DNA topoisomerase I. *J. Biol. Chem.*, **273**, 6050–6056.
10. Zhu,C.-X., Roche,C.J., Papanicolaou,N., Dipietrantonio,A. and Tse-Dinh,Y.-C. (1998) Site-directed mutagenesis of conserved aspartates, glutamates and arginines in the active site region of *Escherichia coli* DNA topoisomerase I. *J. Biol. Chem.*, **273**, 8783–8789.
11. Zhu,C.-X. and Tse-Dinh,Y.-C. (2000) The acidic triad conserved in type IA DNA topoisomerases is required for binding of Mg(II) and subsequent conformational change. *J. Biol. Chem.*, **275**, 5318–5322.
12. Aravind,L., Leipe,D.D. and Koonin,E.V. (1998) Toprim—a conserved catalytic domain in type IA and II topoisomerases, DnaG-type primases, OLD family nucleases and RecR proteins. *Nucleic Acids Res.*, **26**, 4205–4213.
13. Feinberg,H., Changela,A. and Mondragón,A. (1999) Protein–nucleotide interactions in *E. coli* DNA topoisomerase I. *Nature Struct. Biol.*, **6**, 961–968.
14. Perry,K. and Mondragón,A. (2002) Structure of a complex between *E. coli* DNA topoisomerase I and single-stranded DNA. *J. Biol. Chem.*, **277**, 13237–13245.
15. DiGate,R.J. and Marians,K.J. (1989) Molecular cloning and DNA sequence analysis of *Escherichia coli topB*, the gene encoding topoisomerase III. *J. Biol. Chem.*, **264**, 17924–17930.
16. DiGate,R.J. and Marians,K.J. (1988) Identification of a potent decatenating enzyme from *Escherichia coli*. *J. Biol. Chem.*, **263**, 13366–13373.
17. Changela,A., DiGate,R.J. and Mondragón,A. (2001) Crystal structure of a complex of a type IA DNA topoisomerase with a single-stranded DNA molecule. *Nature*, **411**, 1077–1081.
18. Perry,K. and Mondragón,A. (2003) Structure of a complex between *E.coli* DNA topoisomerase I and single-stranded DNA. *Structure*, **11**, 1349–1358.
19. Zhu,C.-X. and Tse-Dinh,Y.-C. (1999) Overexpression and purification of bacterial DNA topoisomerase I. In Bjornsti,M.-A. and Osheroff,N. (eds), *Protocols in DNA Topology and DNA Topoisomerases, Methods in Molecular Biology*. Humana Press, Totowa, NJ, Vol. 34, pp. 145–151.
20. Zumstein,L. and Wang,J.C. (1986) Probing the structural domains and function in vivo of *Escherichia coli* DNA topoisomerase I by mutagenesis. *J. Mol. Biol.*, **191**, 333–340.
21. Wang,Y., Lynch,S., Chen,S.-J. and Wang,J.C. (2002) On the molecular basis of the thermal sensitivity of an *Escherichia coli topA* mutant. *J. Biol. Chem.*, **277**, 1203–1209.
22. Tse,Y.-C., Kirkegaard,K. and Wang,J.C. (1980) Covalent bonds between protein and DNA. Formation of phosphotyrosine linkage between certain DNA topoisomerases and DNA. *J. Biol. Chem.*, **255**, 5560–5565.
23. Laemmli,U.K. (1970) Cleavage of structural proteins during the assembly of the head of bacteriophage T4. *Nature*, **227**, 680–685.
24. Feinberg,H., Lima,C.D. and Mondragón,A. (1999) Conformational changes in *E.coli* DNA topoisomerase I. *Nature Struct. Biol.*, **6**, 918–922.
25. Humphrey,W., Dalke,A. and Schulten,K. (1996) VMD: visual molecular dynamics. *J. Mol. Graph.*, **14**, 33–38.
26. Phillips,J.C., Braun,R., Wang,W., Gumbart,J., Tajkhorshid,E., Villa,E., Chipot,C., Skeel,R.D., Kale,L. and Schulten,K. (2005) Scalable molecular dynamics with NAMD. *J. Comput. Chem.*, **26**, 1781–1802.

27. Baker,N.A., Sept,D., Joseph,S., Holst,M.J. and McCammon,J.A. (2001) Electrostatics of nanosystems: application to microtubules and the ribosome. *Proc. Natl Acad. Sci. USA*, **98**, 10037–10041.
28. Foloppe,N. and MacKerell,A.D.Jr (2000) All-atom empirical force field for nucleic acids. 1. Parameter optimization based on small molecule and condensed phase macromolecular target data. *J. Comput. Chem.*, **21**, 86–104.
29. MacKerell,A.D.Jr and , Banavali,N. (2000) All-atom empirical force field for nucleic acids. 2. Application to molecular dynamics simulations of DNA and RNA in solution. *J. Comput. Chem.*, **21**, 105–120.
30. Eaton,J.W. (2002) *Gnu Octave Manual*. Network Theory Limited, Bristol, UK.
31. Depew,R.E., Liu,L.F. and Wang,J.C. (1978) Interaction between DNA and *Escherichia coli* protein omega. Formation of a complex between single-stranded DNA and omega protein. *J. Biol. Chem.*, **253**, 511–518.
32. Thompson,R. and Cole,P.A. (2001) Probing the mechanism of enzymatic phosphoryl transfer with a chemical trick. *Proc. Natl Acad. Sci. USA*, **98**, 8170–8171.
33. Kim,K. and Cole,P.A. (1998) Kinetic analysis of a protein tyrosine kinase reaction transition state in the forward and reverse direction. *J. Am. Chem. Soc.*, **120**, 6851–6858.
34. Doublie,S. and Ellenberger,T. (1998) The mechanism of action of T7 DNA polymerase. *Curr. Opin. Struct. Biol.*, **8**, 704–712.
35. Cho,H., Wang,W., Kim,R., Yokota,H., Damo,S., Kim,S.H., Wemmer,D., Kustu,S. and Yan,D. (2001) BeF_3^- acts as a phosphate analog in proteins phosphorylated on aspartate: structure of a BeF_3^- complex with phosphoserine phosphatase. *Proc. Natl Acad. Sci. USA*, **98**, 8525–8530.
36. Berger,J.M., Fass,D., Wang,J.C. and Harrison,S.C. (1998) Structural similarities between topoisomerases that cleave one or both DNA strands. *Proc. Natl Acad. Sci. USA*, **95**, 7876–7881.
37. Liu,Q. and Wang,J.C. (1999) Similarity in the catalysis of DNA breakage and rejoining by type IA and IIA DNA topoisomerases. *Proc. Natl Acad. Sci. USA*, **96**, 881–886.
38. Sanner,M.F., Olson,A.J. and Spehner,J.C. (1996) Reduced surface: an efficient way to compute molecular surfaces. *Biopolymers*, **38**, 305–320.